Ochratoxin Binding to Phenylalanyl-tRNA Synthetase: Computational Approach to the Mechanism of Ochratoxicosis and Its Antagonism

Daniel R. McMasters* and Angelo Vedani

Biographics Laboratory 3R, Missionsstrasse 60, CH-4055 Basel, Switzerland

Received March 16, 1999

Ochratoxin A (OA) is a toxic isocoumarin derivative released by various species of mold which grow on grain, coffee, and nuts, representing a serious worldwide health problem. Among other mechanisms of toxicity, it has been suggested that OA inhibits phenylalanyl-tRNA synthetase (PheRS), thereby reducing protein synthesis. Using the crystal structure of PheRS from *Thermus thermophilus*, we have modeled its interactions with OA as well as with phenylalanyl adenylate (FAMP), the high-affinity intermediate substrate of PheRS. Our results indicate that while OA may be capable of weakly inhibiting PheRS, the OA−PheRS complex cannot adopt the same conformation as does FAMP−PheRS, contrary to previous assumptions. Relative to FAMP, the phenylalanyl moiety is found to bind more shallowly and in a different overall conformation. Free-energy perturbation calculations of the relative free energies of binding of OA with the phenolic moiety protonated versus deprotonated suggest that the protonated form binds significantly more strongly. Two alternative binding modes were also identified which cannot be discounted on the basis of these calculations. Our results, however, do not suggest binding stronger than millimolar for any of the binding modes, a conclusion which is in agreement with more recent experimental findings. This, in turn, suggests that the previously observed antagonistic effects of aspartame and piroxicam are more likely due to their prevention of OA binding to human serum albumin than to PheRS, which is in agreement with binding studies as well as with preliminary simulations performed in our laboratory.

Introduction

Ochratoxins are a class of small organic molecules produced and released by various species of mold such as *Aspergillus alutaceus* and *Penicillin verrucosum*.[1,2] Ochratoxins are a nearly ubiquitous contaminant of grain, coffee, and other crops and represent a serious health threat both to humans and to livestock in many areas of Europe, North America, Asia, and Africa. Their toxic effects include carcinogenicity, mutagenicity, and nephrotoxicity. With regard to the latter, they have been implicated in the etiology of Balkan endemic nephropathy, an often fatal kidney failure observed in the Balkans.[3]

The primary culprit in ochratoxicosis is ochratoxin A (OA).[4] Chemically, OA is composed of a substituted isocoumarin linked to L-phenylalanine. It has been speculated that deprotonation of the phenolic moiety on the isocoumarin may be involved in the toxic mechanism of ochratoxins. This may be related to either the absorption, elimination, or binding properties of ochratoxin. Chu has observed a correlation between the toxicity of several ochratoxins and the pK_a of their phenolic proton, OA and OC having the lowest pK_a and the highest toxicity.[5] OB, for example, has a pK_a approximately 1 unit higher than OA and is approximately 10 times less toxic. The pK_a of the phenolic group of OA is near 7 (it has been reported as 7.1 and as 6.75),[6,7] indicating that the compound is present in solution as both the monoanion (OA^-, in this work referred to simply as OA) and the dianion (OA^{2-}) in substantial quantities at physiological pH. In this work, therefore, we examine both of these ionization states.

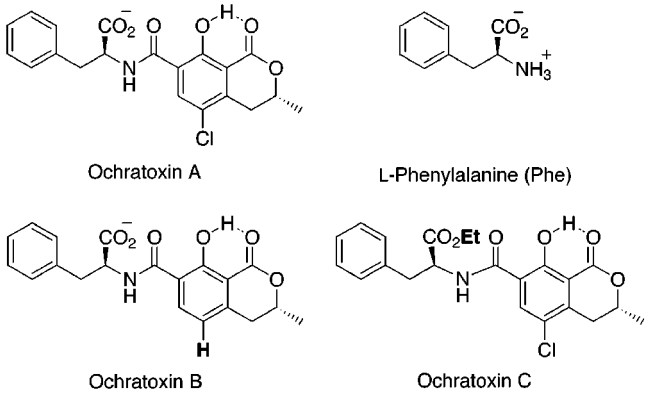

The pK_a of the carboxylic acid moiety, on the other hand, is apparently much lower; the neutral toxin (OA^0) is probably not present in vivo to any appreciable extent, except in the gastrointestinal tract, where it may be relevant during absorption.

Since its discovery in 1965,[8] much research has been conducted with the goal of elucidating the toxic mechanism of OA. Toxicological data point to a number of effects of OA in vivo, including inhibition of protein synthesis, induction of lipid peroxidation, and inhibition of mitochondrial ATP production, but consensus as to which effect or effects represent the primary mechanism of ochratoxicosis is yet to be reached.[2]

The presence of an L-phenylalanine (Phe) moiety in the structure of OA raised the suspicion early on that inhibition by OA of Phe-metabolizing enzymes may be responsible for the toxic effects of the former in vivo. One of the first reports supporting this hypothesis

10.1021/jm991040k CCC: $18.00
Published on Web 07/16/1999

experimentally was from Konrad and Röschenthaler, who measured the inhibition of phenylalanyl-tRNA synthetase (PheRS, also known as phenylalanine tRNA: ligase) from *Bacillus subtilis* (PheRSBS) in the charging of phenylalanyl-tRNA ($tRNA^{Phe}$) by OA.[9] From their data, they derived Michaelis and inhibition constants of 1.3×10^{-6} and 3.0×10^{-6} M, respectively, when using $tRNA^{Phe}$ from *B. subtilis* and $K_m^{Phe} = 1.3 \times 10^{-6}$ M and $K_i = 3.5 \times 10^{-5}$ M when using *Escherichia coli* $tRNA^{Phe}$. No inhibition was observed, however, when using PheRS from *E. coli* (PheRSEC).[10,11]

Subsequently, the group of Creppy investigated this phenomenon using PheRS from yeast, *Saccharomyces cerevisiae* (PheRSSC).[12] The data obtained by Creppy et al. for K_m^{Phe}, namely 3.3×10^{-6} M, was close to that of Konrad and Röschenthaler, but the observed $K_i = 1.3 \times 10^{-3}$ M was substantially higher. This indicates that OA is incapable of competitively inhibiting an equimolar concentration of Phe, leading these authors to speculate either an intracellular enrichment of OA or inhibition of PheRS by an OA metabolite to explain the in vivo toxicity of OA.

In 1993, Roth and co-workers repeated the experiments of Konrad and Röschenthaler using specially purified PheRSBS and obtained values of $K_m^{Phe} = 2.8 \times 10^{-5}$ M and $K_i^{Phe} = 4.33 \times 10^{-3}$ M.[13] These data, viewed alone, would seem to support the in vivo inhibition of PheRS by OA more so than the results of Creppy et al. However, Roth et al.'s measurement of the intracellular concentrations of OA and Phe, while demonstrating a 20-fold enrichment of OA, revealed concentrations of $[Phe] = 3 \times 10^{-4}$ M and $[OA] = 1 \times 10^{-3}$ M. From these data, the percent inhibition is calculated to be a mere 2%.[12] Thus, Roth et al. dismiss the hypothesis that competitive inhibition of PheRS by OA is responsible for the latter's toxicity. This view is shared by Bruinink et al., who observe that OA is toxic to cell cultures at the submicromolar level, several orders of magnitude below the concentrations necessary to elicit PheRS inhibition.[14] Creppy et al., on the other hand, have reported the measurement of a much higher intracellular OA concentration of 2.7×10^{-2} M.[15]

Interestingly, the values obtained by Creppy et al. and by Roth et al. for K_i (which equals the dissociation constant K_d in the case of competitive inhibition) are similar, yet the authors come to opposite conclusions regarding the relevance to ochratoxicosis. Summing up the available data, it appears uncontested that OA binds weakly to moderately to PheRS, with reported dissociation constants 3.0×10^{-6} M $\leq K_d \leq 4.3 \times 10^{-3}$ M. The question as to the OA−PheRS binding mode remains, however, unanswered. In fact, it remains all but unasked. It has been hitherto assumed, due to OA's Phe moiety, that OA binds analogously to Phe itself, with the Phe moiety in the Phe-binding pocket of PheRS.

It has proven virtually impossible to control the growth of ochratoxin-producing molds in stored foods. Therefore, other means of lessening the deleterious effects of these compounds have been investigated, such as destruction of the toxin by irradiation or heating, more careful food testing for contamination, or in vivo ochratoxin antagonists. Recently, the artificial sweetener aspartame was proposed as an ochratoxin antagonist.[16] Its major mechanism of action was believed to be prevention of ochratoxin-induced inhibition of protein synthesis, although it was unclear whether this antagonism should be ascribed to aspartame itself or to Phe produced by the metabolism of aspartame, which yields Phe, aspartic acid, and methanol. The recent suggestions that PheRS may not be involved in ochratoxicosis,[13,14] however, indicate that aspartame may have a different mode of antagonism. Indeed, Baudrimont et al. found that aspartame inhibits the binding of OA to plasma proteins, an effect also observed with the nonsteroidal antiinflammatory drug piroxicam.[17] This may allow the toxin, which typically has a half-life in vivo of 3−5 weeks (monkey),[18] to be washed more quickly from the body, with concomitant decrease in overall toxicity. Kumagai et al. have shown that the half-life of OA is much shorter in albumin-deficient rats than in normal rats, demonstrating the importance of binding to plasma proteins on ochratoxin toxicokinetics.[19]

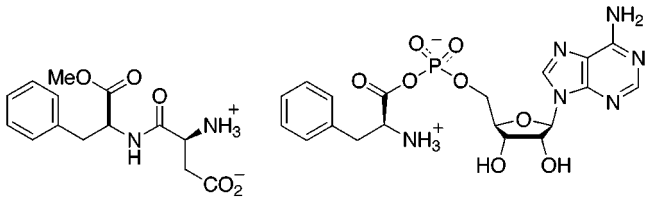

Aspartame Phenylalanyl adenylate (FAMP)

In the search for more effective antagonists, it is crucial to understand the mechanism by which known antagonists act. In light of the scope of this problem and the discrepancy in the literature with respect to the most promising targets for antagonizing ochratoxicosis, we felt that an examination of OA−PheRS interactions on a *molecular basis* is timely. We have therefore investigated these interactions using the recently available X-ray crystal structure of PheRS[20] and present our findings here. Because OA also binds extensively to human serum albumin (HSA) in vivo, it is likewise necessary to examine OA−HSA interactions in order to fully assess the action of candidate antagonists. Some qualitative and therefore preliminary observations with respect to OA−HSA are also presented.

Experimental Section

Generation of Reference Structures of the Ligands. The structures of OA, OA^{2-}, phenylalanyl adenylate (FAMP), and aspartame were generated using the modeling software MacroModel version 5.0.[21] The structure of each compound was minimized in implicit aqueous solvent[22] using the AMBER force field[23] as implemented in MacroModel. A Monte Carlo conformational search was performed using default charges. The atomic partial charge model of the lowest-energy conformer was then calculated by fitting the electrostatic potential, calculated from the MNDO wave function, using the ESP algorithm[24] as implemented in MOPAC version 6.[25] The ESP-derived charges for the ligands were left unaltered throughout all simulations.[26]

Generation of the Starting Conformation of PheRS. The coordinates of the α-subunit of phenylalanyl-tRNA synthetase from *Thermus thermophilus* (PheRSTT)[20] were obtained from the Brookhaven Protein Data Bank[27] (structure code 1PYS, resolution = 2.9 Å) and fully refined in aqueous solution with MacroModel before proceeding. The protonation states of His, Glu, and Asp residues were assigned with the aid of the "Hydpos" module in the Yeti software.[28a] Docking of the ligands, including manual adjustment of individual residues, was performed using PrGen 2.0.[28b] Simulations of the

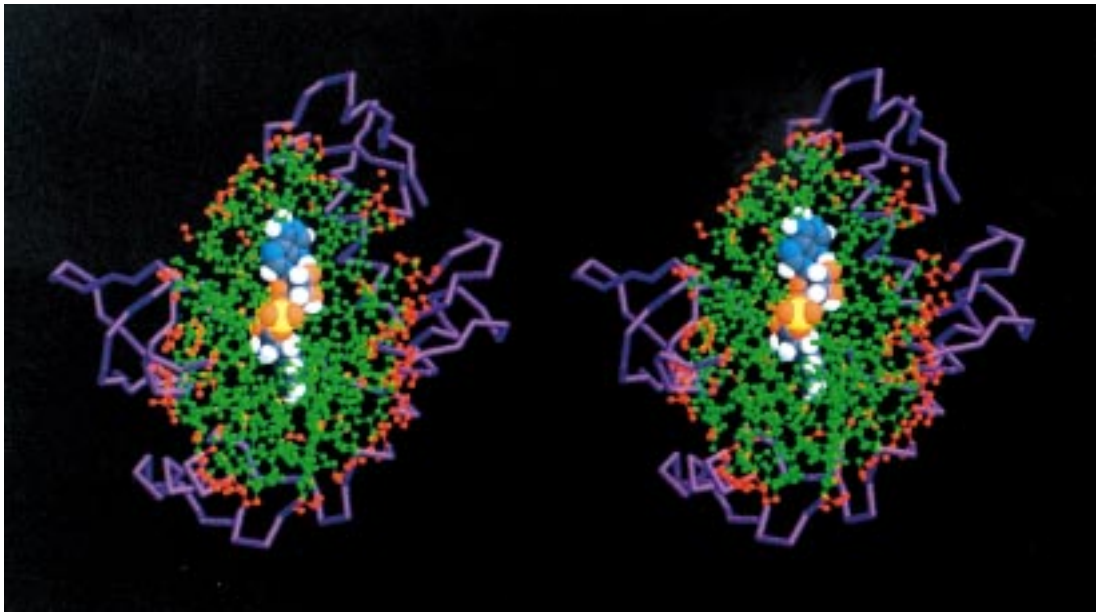

Figure 1. Stereoview of PheRSTT showing the zones used in the molecular dynamics simulations: the ligand (here, FAMP, CPK model) and a 12 Å zone of the protein (green ball-and-stick model) were allowed to move freely; a further 3 Å shell (red ball-and-stick model) was constrained with a harmonic restoring force. The rest of the protein (purple backbone model) was ignored in the molecular dynamics simulations. Figures 1, 4, and 6 were created using RasMol (ref 50).

enzyme were performed using united carbon atoms, but with explicit polar hydrogen atoms; MNDO/ESP charges were retrieved from the AMBER database for the protein. All simulations were performed with implicit aqueous solvent using the GB/SA algorithm and with extended nonbonded cutoff distances of 20 Å for Coulombic and 8 Å for van der Waals interactions. The three-dimensional coordinates of the various structures presented in this article can be requested at www.biograf.ch.

Molecular Dynamics Conformational Search. The entire tetrameric protein is too large to be simulated with the resources available to us, nor could the cognate tRNA be considered. To sample the conformational space available to the complexes formed with PheRS, yet avoid straying too far from the experimental structure found for the full tetramer,[29a] molecular dynamics simulations were performed on a "hot zone" consisting of a 12 Å zone of PheRS around the ligand OA which was completely free, which in turn was surrounded by a 3 Å zone of atoms constrained to their initial positions with a 100 kcal·mol^{-1}·Å^{-2} harmonic constraint function, an approach used previously in studies of the green fluorescent protein.[29b] Any atoms falling outside these zones were ignored in these simulations. The various zones used in the molecular dynamics simulations are shown in Figure 1. After docking and manual adjustment of small-molecule and protein side-chain conformations using PrGen 2.0, the structures were subjected to molecular dynamics; intermediate structures were stored for subsequent minimization. Typically, 10 ps of dynamics were performed at 750 K, and 10 structures were sampled during this time, each of which was minimized. In addition, simulated annealing was performed following the 10 ps equilibration period, allowing the system to cool from 750 to 50 K over 40 ps. The lowest-energy structures were inspected visually for possible favorable conformational changes, such as rotation of individual residues to maximize interaction with the ligands. The resulting structures were then resubjected to dynamics and minimization, this time at 300 K. The dynamics simulations were thus performed using a two-tiered approach: high-temperature simulations at 750 K allowed major conformational changes, to search for new binding modes. These were then followed by simulations at 300 K, which allowed for local conformational changes and full relaxation. In the case of FAMP, whose general mode of binding was already known (vide infra), initial simulations were performed at 300 K instead of at 750 K, to explore only small changes in the local binding.

The best conformations found in the simulations of the binding-site zone were then minimized relaxing the entire α-subunit. This served above all to remove any strain between the movable zone and the rest of the protein which may have developed during the molecular dynamics simulation; no major conformational changes were observed during this step.

The molecular dynamics simulations served to explore the flexibility of side chains of the residues lining the active site. To increase the probability of rearrangement of those side chains, initial molecular dynamics simulations were performed at 750 K. In addition, several of the larger residues, such as Arg321 and Gln218, were adjusted manually, to ensure that more than one conceivable conformation was sampled. In addition to the conformational flexibility, the protonation state of the active-site side chains is important in the modeling. Analysis based on directional interactions (vide supra) within the protein identified His178 as potentially δ- or ϵ-protonated; both of these possibilities were explored with molecular dynamics.

Free-Energy Perturbation Simulations. FEP simulations were also performed with MacroModel using the AMBER force field, GB/SA implicit aqueous solvent, and extended nonbonded cutoffs. The simulations were performed over 21 perturbation windows ($\Delta\lambda = 0.05$), each window consisting of 5 ps equilibration time and 5 ps sampling time, using the mixed Monte Carlo/stochastic dynamics algorithm[30] and sampling in both directions. For the complexes, a 10 Å zone around the ligand was allowed to move freely, while the atoms in a further 3 Å shell were constrained to their original positions with a 100 kcal·mol^{-1}·Å^{-2} harmonic restoring force; the remaining atoms of the protein α-subunit were included in the nonbonded list, but their positions were invariant.

Results

As a first step, FAMP, the natural high-affinity substrate of PheRS, was docked into the Phe binding site of the enzyme. The location of this active site is known unambiguously from the crystal structure of PheRSTT complexed with its cognate tRNA (tRNA^{Phe}),[20] the CCA 3′-terminus of which must reach into the active site. The high degree of homology among class II tRNA

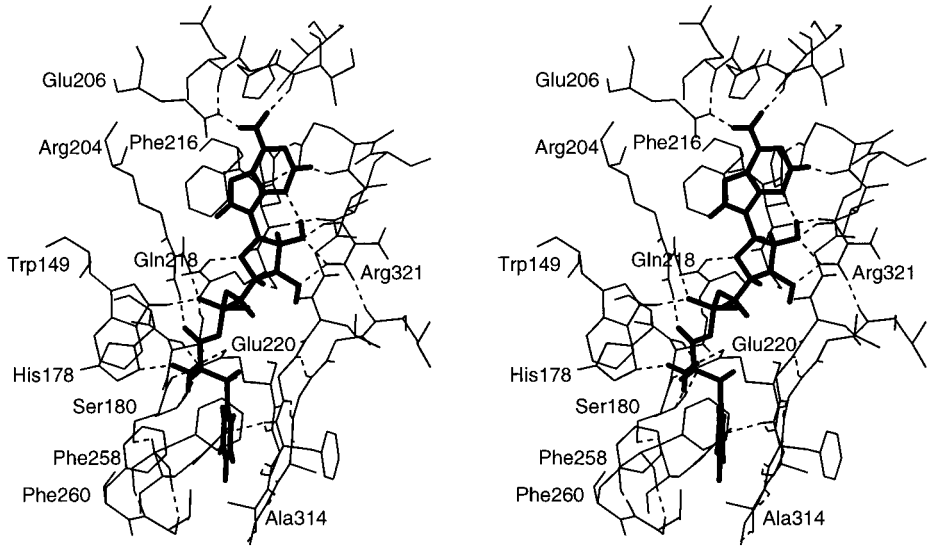

Figure 2. Stereoview of FAMP bound in the active site of PheRSTT.

synthetase binding sites,[31] together with the X-ray crystal structures of histidyl-tRNA synthetase with histidyl adenylate (HAMP) bound[32] and lysyl-tRNA synthetase with lysine bound,[33] also leaves no doubt as to its location. The binding site is located on the α-subunit of the enzyme, a catalytic $(\alpha\beta)_2$ tetramer, and is lined by an extended antiparallel β-sheet structure, as well as shorter helical domains and turns (Figure 1). FAMP could be docked in a conformation analogous to that of HAMP in HisRS after some adjustment of the side chains of residues defining the active site. Minimization and simulated annealing dynamics simulations then succeeded in adapting the ligand and enzyme optimally to one another.

As can be expected based on the experimentally determined strong binding of FAMP to PheRSSC, $K_d = 4 \times 10^{-9}$ M,[34] numerous specific interactions were identified between the enzyme and substrate (Figure 2). The phenyl group is enclosed snugly within a hydrophobic pocket, lined on one side by Phe258, Phe260, Ala314, and Val261 and on the other side by the antiparallel β-sheet structure. The *para* carbon atom of the phenyl group is located within 3.6 Å of the β-carbon of Ala314, consistent with the finding that this residue is decisive in the discrimination of Phe from unnatural amino acids *p*-Cl-phenylalanine and *p*-Br-phenylalanine.[35,36] In addition to the salt bridge with the class II-conserved acidic residue Glu220, the ammonium group forms H-bonds to His178, which is ϵ-protonated when FAMP is bound, and Ser180. The phosphate group of FAMP interacts with Arg204, invariant among all class II RSs, Trp149, and solvent, while the carbonyl group has contacts with Arg204 and Gln218. Gln218 forms an additional H-bond to the ribose ring oxygen atom of FAMP, as well as to Thr179. The ribose hydroxyl groups interact with Arg321, also a conserved residue. Finally, the adenine forms H-bonds with the backbone carbonyl of Thr211, forms van der Waals contact with Ile332, and is stacked against Phe216, also nearly invariant. The geometries of the hydrogen bonds formed between FAMP and PheRSTT are summarized in Table 1. The binding of FAMP to PheRSTT is thus marked by the same patterns seen in other class II tRNA synthetases, such as HAMP−HisRS.[11,32]

Table 1. Selected Polar Interactions of FAMP and OA with PheRS[a]

	residue	*d* (Å)	*θ* (deg)	*ω* (deg)
	Ligand = FAMP			
adenine NH_2	Glu206	1.79	155	23
	Thr211	1.83	160	18
adenine N	FAMP (ribose 2′-OH)	1.98	161	46
ribose 2′-O	Arg321	1.88	143	24
	Arg321	2.07	136	26
ribose 3′-O	Arg321	1.92	141	25
ribose ring O	Gln218	2.01	143	16
$P-O^-$	Arg204	1.76	161	19
	Trp149	1.74	161	3
C=O	Arg204	1.85	141	4
NH_3^+	Glu220	1.73	161	31
	Glu220	2.09	127	45
	Ser180	1.89	139	33
	His178	1.91	146	31
	Ligand = OA; Orientation = Phe Buried			
CO_2^-	His178	1.78	146	40
	Arg204	1.77	157	8
	Arg204	1.76	152	48
	Trp149	1.69	166	37
C=O (amide)	Gln218	1.77	166	37
	OA (phenol H)	1.77	139	35
phenol O	Arg321	2.02	130	17
C=O (lactone)	Arg321	1.90	144	25
	Arg321	1.83	151	45
	Ligand = OA; Orientation = Phe Exposed			
C=O (lactone)	Thr179 backbone	1.88	143	34
	Thr179 side chain	1.81	159	46
	OA (phenol H)	1.96	131	43
phenol H	Gln218	1.87	137	33
phenol O	OA (amide NH)	1.92	126	19
CO_2^-	OA (amide NH)	1.95	114	35
	Gln218	1.80	152	51
	Trp149	1.79	142	60
	Arg204	1.64	178	11
	Arg204	1.69	162	30
	Ligand = OA; Mode = Loose Binding Site			
C=O (lactone)	OA (phenol H)	1.83	138	35
phenol O	OA (amide NH)	2.09	120	27
C=O (amide)	Arg204	1.80	148	56

[a] *d* = donor−H···acceptor distance; *θ* = donor−H···acceptor angle; *ω* = angle to closest acceptor lone pair, H···acceptor−lone pair.

Docking of OA into the binding site of PheRS was then performed. As a first attempt, the entire phenylalanine moiety of OA was superimposed onto that of FAMP, in accord with the prior assumption that the two

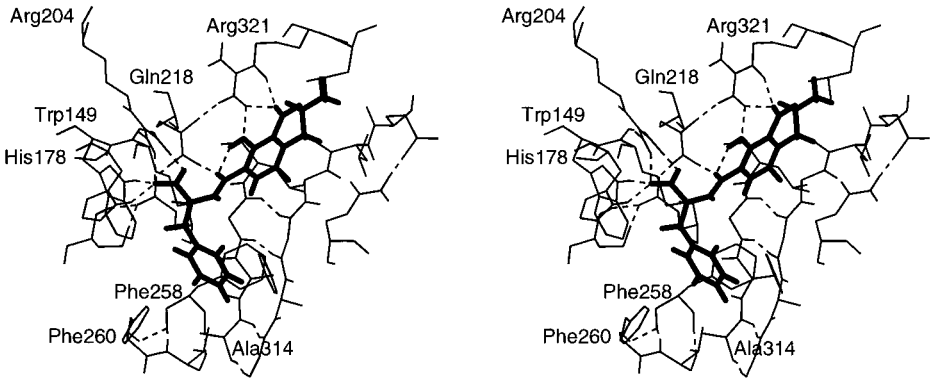

Figure 3. Stereoview of OA bound in the active site of PheRSTT.

ligands bind analogously. Comparison of their three-dimensional structures reveals an important difference, however. In the case of FAMP, the phenylalanine moiety is substituted at the carboxylic acid; in OA, however, it is the amino group which bears the substituent. As a result, the phenylalanyl moiety of OA cannot be brought into superposition with that of FAMP, as this would require the isocoumarin moiety to protrude well out of the binding pocket, into a region of space already occupied by the bulk enzyme. Thus, in the absence of major enzyme reorganization (in which case no simple assumptions can be made about the binding mode and associated changes in energy), the previous hypothesis of analogous binding modes is untenable.

A further difference between the Phe moiety of FAMP and that of OA involves the charge distribution. Whereas FAMP has a formal positive charge at the nitrogen and a formally neutral carbonyl group, in OA it is the nitrogen which is formally electroneutral and the carboxylate is negatively charged. By retaining the phenyl group of OA superimposed with FAMP's phenyl group and rotating the Phe $\alpha-\beta$ bond of OA by approximately 180°, docking is possible with minor adjustments of the protein side chains. The conformation obtained, however, has H-bond donors and acceptors in different positions relative to FAMP. The carboxylate group, for example, points away from the basic groups Arg204 and Gln218 and into the hydrophobic pocket, where no hydrogen-bond donors or electropositive groups are available to compensate the energy of desolvating this charged group. Thus, not even the phenyl group can be reasonably expected to bind in the same position in OA as in FAMP.

Nevertheless, by adjusting the conformation of the ligand and some side-chain residues of the protein (scanning the Ponder−Richards rotamer library[37] as implemented in PrGen[28]), it was possible to dock OA into the protein with the phenyl group buried in the hydrophobic pocket. This OA−PheRS complex was subjected to molecular dynamics and minimization, to allow the enzyme to adapt to OA (see Experimental Section for details). Indeed, several low-energy conformations were found, none of which however was as low in energy as the FAMP−PheRS complex depicted in Figure 1. In the lowest-energy conformation found, the following interactions are observed (Figure 3, Table 1): The phenyl group of the Phe moiety occupies the hydrophobic pocket; however, it is situated more shallowly than FAMP, as shown in Figure 4. The distance between the methyl carbon atom of Ala314 and the ligand phenyl *para* carbon atom is 3.6 Å for FAMP; for OA it is 4.2 Å. Furthermore, whereas the phenyl group of FAMP lies essentially flat against the β-sheet wall ($\angle \approx 10°$), maximizing van der Waals contact, in this conformation of OA, the phenyl group makes an angle of approximately 30° with the wall. As a result, the phenyl group of FAMP forms favorable van der Waals interactions with the protein 6.2 kJ·mol^{-1} stronger than does that of OA in this binding mode. The carboxylate group interacts with Arg204, His178, and Trp149. These strong polar interactions are responsible for the shallow fit of the phenyl group in the hydrophobic pocket, the ligand having to slide out slightly to enable the carboxylate to reach Arg204. The isocoumarin moiety also leans against the β-pleated sheet, and Arg321 forms H-bonds to the lactone moiety and phenolic oxygen. Finally, Gln218 forms an H-bond to OA's amide carbonyl. The less polar region of the isocoumarin moiety, including the chlorine atom and methyl group, contacts the β-sheet on one side but is exposed to solvent on the other.

Interestingly, the lowest-energy structure found for the ochratoxin dianion bound to PheRS (PheRS−OA^{2-}) has a conformation almost identical to that of the monoanion (PheRS−OA^{-}, Figure 3). Removal of the phenolic proton results in the loss of an intramolecular H-bond to the amide carbonyl but also allows Arg321 to interact more strongly with the two exocyclic oxygen atoms, forming a salt bridge. Despite the fact that the various components of the total energy are very different for the two compounds (especially the electrostatic and solvation contributions, due to the different charge distributions), the overall minimized energies are nearly identical.

To distinguish between these two ionization states, free-energy perturbation calculations were performed. In these calculations, the monoanion was converted, slowly and reversibly, into the dianion, first free in aqueous solution and then bound to PheRS. The results are listed in Table 2. The total free-energy difference was in both cases quite large due to the large change in solvation energy which accompanied the change in overall charge of the ligand. This required that the simulation be performed with many small windows ($\Delta\lambda = 0.05$/window) in order to avoid changes much greater than 5 times kT per window,[38] which made the calculation more costly. Due to limited computational resources, the FEP simulations had to be performed using

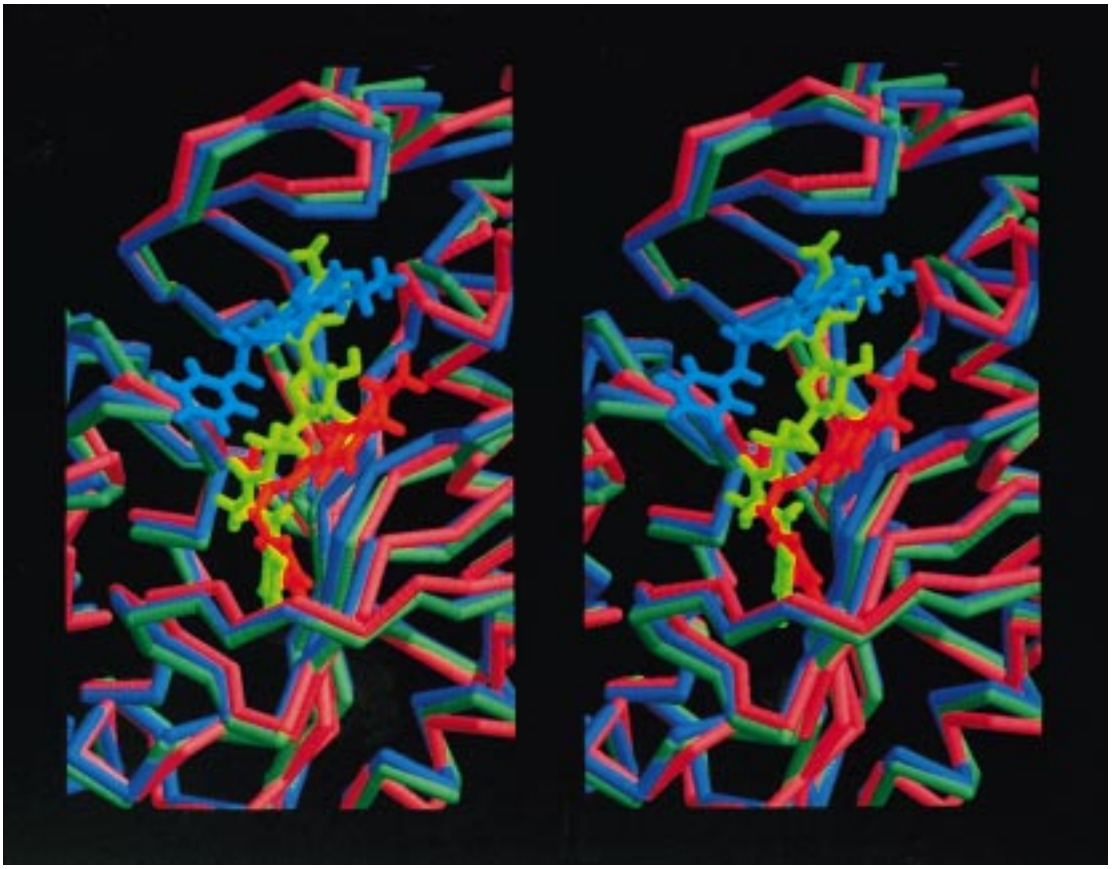

Figure 4. Stereoview of the minimized structures of PheRS: with FAMP bound (green), with OA bound (red), and with OA bound in the alternate subsite (blue).

Table 2. Results of FEP Simulations of OA and OA^{2-}

	$OA^- \rightarrow OA^{2-}$	
	aqueous solution	bound to PheRS
ΔG (kJ·mol^{-1})	-202.6 ± 0.8	-166 ± 2
$\Delta\Delta G$ (kJ·mol^{-1})	37 ± 2	

a slightly smaller zone than for the normal dynamics simulations (vide supra). As has been pointed out by van Gunsteren,[39] the use of a constrained zone (extended wall region boundary condition) in FEP simulations can lead to increased systematic error, especially in cases where atoms or residues are created or annihilated during the simulation, because the simulation no longer occurs at constant pressure. In the present case, the annihilation of a proton, exposed to the (implicit) solvent, would not seem to change the steric environment within the binding site significantly. Nevertheless, we did observe a dependence on the zone size, which however correlated strongly with the overall charge of those atoms of the protein included within the zone, as determined by a zone-dependence study performed upon a single FEP window ($0.48 \leq \lambda \leq 0.52$). This is not surprising considering the large magnitude and long range of Coulombic interactions, together with the fact that charge was created during the run. To include the effect of the charge distribution of the protein, without having to pay the prohibitive computational price of simulating the full protein, those atoms lying outside the zone were held frozen. This caused them to be included in the nonbonded list but did not require their motion to be calculated. In this way, the zone-size dependence was decreased significantly. The presence of the β-subunit or of the highly negatively charged $tRNA^{Phe}$, however, may influence these findings. Although the requirements of many perturbation windows and inclusion of the entire protein α-subunit limited the simulation sampling time to 5 ps/window, the use of the mixed Monte Carlo/stochastic dynamics algorithm[30] helped to speed convergence. The result of the FEP simulation of the free ligands in solution was the same when performed with a sampling time of 5 ps/window as with 1000 ps/window (-202.6 ± 0.8 vs -202.6 ± 0.3 kJ·mol^{-1}). A single window ($0.45 \leq \lambda \leq 0.55$) of the complex was examined for 100 ps and showed variations in ΔG an order of magnitude smaller than the difference $\Delta\Delta G$ between the complex and the free ligand in this window; the final ΔG was also nearly the same after 100 ps as after 5 ps (-16.32 vs -16.51 kJ·mol^{-1}).

The calculated $\Delta\Delta G = 37 \pm 2$ kJ·mol^{-1} indicates that although the dianion is more abundant at physiological pH, the monoanion displays the higher affinity to PheRS. This finding does not rule out the importance of the pK_a of the phenolic moiety in ochratoxin toxicity; as pointed out earlier, the dianion could be relevant in absorption, elimination, or binding properties. Indeed, it has been found that ochratoxin B is more rapidly hydrolyzed by bovine carboxypeptidase A than OA.[40]

Because OA cannot bind analogously to FAMP, and considering that it is a relatively small, flexible molecule, other binding modes are conceivable, and several

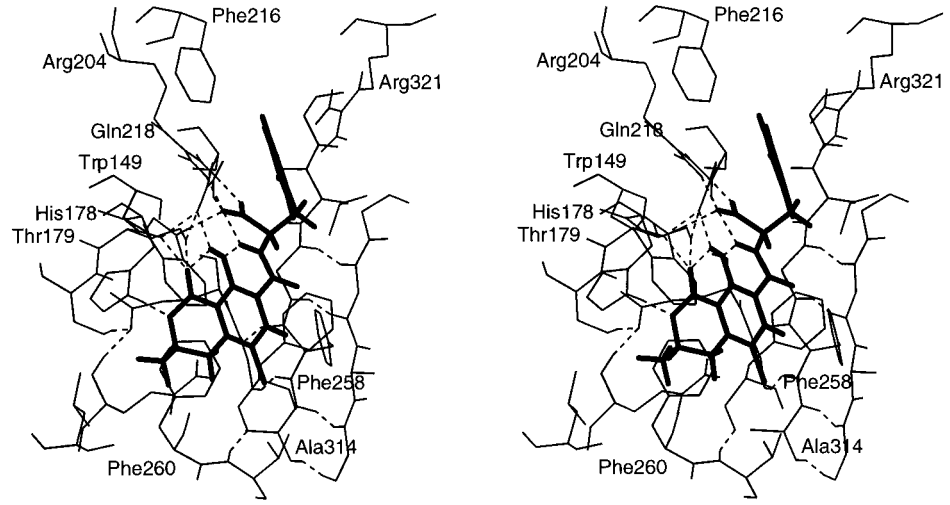

Figure 5. Stereoview of OA bound in the active site of PheRSTT in the "Phe-exposed" mode.

alternative binding orientations were also considered. The molecular dynamics simulations, while allowing substantial reorganization of amino acid residues and ligand conformation, were far too short to simulate the change in orientation necessary to examine alternative binding modes, especially considering that such a change would probably require dissociation, rotation of the entire ligand, and redissociation, a process unlikely to occur on the subnanosecond time scale accessible with our simulations. OA was therefore manually docked in a reverse mode, oriented 180° from the "Phe-buried" mode described above, with the isocoumarin moiety nestled in the hydrophobic pocket which normally encloses the phenyl group of the natural substrate. Because the isocoumarin group is somewhat bulkier than a phenyl group, it cannot be easily accommodated in the binding pocket in the minimized structure of the complex (FAMP−PheRS). However, only a small amount of "breathing" is necessary to make room for the isocoumarin moiety; the energy associated with the expansion of the binding pocket was of course taken into account in the subsequent minimization and molecular dynamics.

Low-energy conformers were identified by molecular dynamics simulations in this reverse mode also. In the most stable conformer found for this orientation (cf. Figure 5 and Table 1), the hydrophobic pocket, especially residues Phe258 and Phe260, interacts with the methyl group and chlorine atom of the isocoumarin moiety. The carboxylate of OA is situated approximately where the phosphate group of FAMP binds to Arg204, forming a salt bridge, and has additional contacts with Trp149 and Gln218. The amide carbonyl oxygen atom is solvent-accessible, and the isocoumarin carbonyl oxygen atom forms H-bonds with Thr179.

Although the estimated energy of this binding mode lies above that of the previously discussed "Phe-buried" mode, the use of a substructure zone artificially constricted the binding site to the conformation in the crystal structure, which was determined with tRNA bound but with no ligand in the Phe binding site. Therefore, a full-structure minimization was necessary to estimate better the true energetic cost of expanding the binding site. Indeed, following the full-structure minimization, the energy of this conformer is comparable to that of the overall lowest-energy, "Phe-buried" conformer.

In addition, we identified a second subsite of PheRS where OA binding might occur. In this conformation, OA is positioned where the adenine moiety of FAMP binds (Figure 4). Thus, in the lowest-energy conformation found for this binding mode, the isocoumarin moiety occupies the adenine binding pocket, surrounded by Phe216, Ile332, Met324, and Arg321. A hydrogen bond is formed between Arg204 and the amide carbonyl oxygen of OA, and the phenyl group leans against Met148 (Table 1). This binding mode is marked by relatively few strong contacts between the ligand and the enzyme, which suggests weak binding, as observed experimentally by Roth et al. and Creppy et al.[12,13]

Additional sites may exist on the periphery of the tetrameric enzyme where OA could weakly bind, analogously to this site. The virtue of this site is that it could explain the antagonistic action of aspartame on OA toxicity. In this mode, OA occupies the adenine binding pocket, thereby preventing the binding of ATP and its subsequent reaction with Phe, thereby inhibiting protein synthesis. Aspartame could bind in a conformation which blocks OA binding but does not overlap with FAMP, thus antagonizing the inhibition by OA without itself disturbing protein synthesis. We cannot yet conclude whether this mode is that which occurs in nature, nor even if the beneficial effects of aspartame on ochratoxicosis are due to such a "selective displacement" mechanism. The observation of this possible binding site, however, suggests the use of such a strategy in designing toxin antagonists. We are currently investigating the possibility of selective displacement in diminishing the effects of ochratoxicosis with respect to human serum albumin (HSA). On the basis of our results and a review of the literature, we feel that HSA may be the more important target for ochratoxin antagonists (see Discussion section below).

HSA is a versatile transport protein which binds a wide range of small acidic compounds,[41] including OA,[18,42,43] thereby representing an additional target for prospective ochratoxin antagonists. The three-dimensional structure of HSA, which is notable for its high

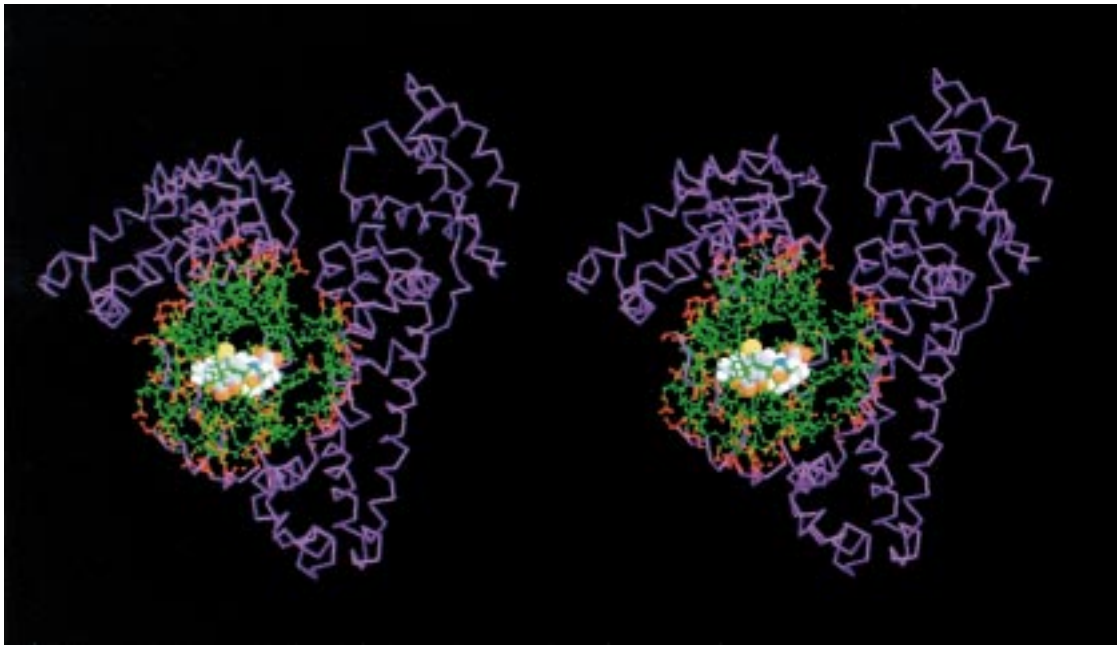

Figure 6. Stereoview of HSA with OA bound, showing the zones used in the molecular dynamics simulations (cf. Figure 1).

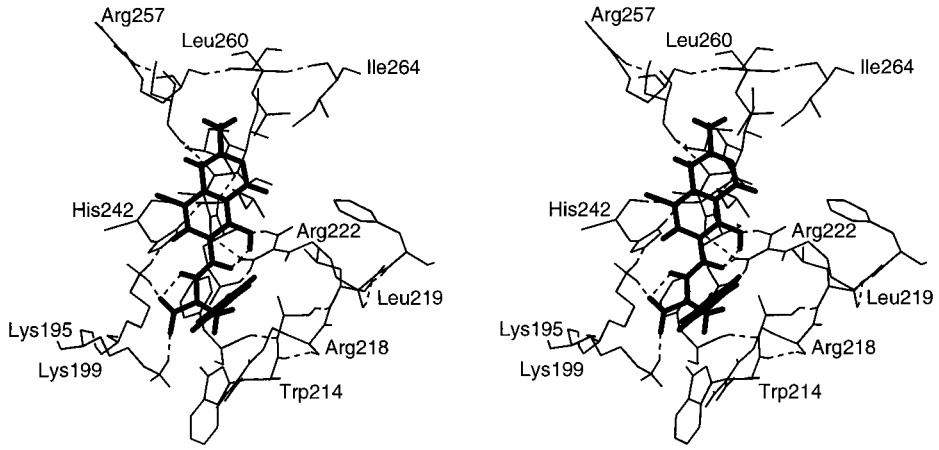

Figure 7. Stereoview of OA bound in subdomain IIA of HSA.

α-helical content and large number of interhelical disulfide bridges, has recently been made available at the Brookhaven Protein Data Bank,[44] and we are currently investigating its interaction with OA; we have begun by examining the binding of OA to HSA's subdomain IIA, the warfarin binding site. Figure 6 depicts the regions of HSA included in the molecular dynamics simulation of the warfarin binding site. This binding site can be described as a cage of α-helices and is lined

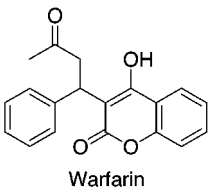

Warfarin

with several basic and numerous hydrophobic residues. Warfarin and OA share some structural similarities, and preliminary simulations suggest a similar binding mode for these two compounds in the IIA binding site, the phenyl groups and (iso)coumarin moieties occupying the same subpockets. In the lowest-energy conformation found for OA in the IIA binding site (Figure 7), obtained from over 1 ns of dynamical simulation, the isocoumarin of OA is located where the phenyl ring of 2,3,5-triiodobenzoic acid (TIB) binds, as determined by X-ray crystallography.[44] The carboxylate group of OA also adopts an orientation similar to that of the carboxylate group of TIB, forming a strong polar interaction with Lys199. The phenyl group of OA is enclosed in a hydrophobic subpocket, sandwiched between Trp214 and Arg218 on one side and Phe211 and His242 on the other, and surrounded by additional hydrophobic residues Leu219, Leu238, and Ala215. The principal polar interactions are listed in Table 3.

Discussion

The accurate quantitative estimation of binding affinities between proteins and small molecules, despite the advances of the past decades, remains a challenge. Generally, such calculations depend on the affinity being known for one or more similar compounds. The dissociation constant of interest can then be calculated

Table 3. Selected Polar Interactions of OA with HSA[a]

	residue	d (Å)	θ (deg)	ω (deg)
	Ligand = OA			
CO_2^-	Lys195	1.76	156	15
	Lys199	1.67	167	55
	OA (amide NH)	1.92	115	30
C=O (amide)	Arg222	1.86	151	47
	OA (phenol H)	1.80	135	48
phenol O	Arg222	1.84	157	23
	Ligand = TIB (from ref 44)			
CO_2^-	Lys199			
	Arg222		not reported	
	Arg257			

[a] d = donor−H···acceptor distance; θ = donor−H···acceptor angle; ω = angle to closest acceptor lone pair, H···acceptor−lone pair.

directly using free-energy perturbation or indirectly using 3D-QSAR methods.

In the case of OA−PheRS, two different values appear in the literature for the binding affinity of OA, whereas no data are available for related compounds. In this case, a calibration of the predicted binding affinity with experimental data is restricted to comparison with FAMP and the assumption that the lowest-energy conformers have been identified. Although a conformation is available to the complex in which all of the polar groups of OA are engaged in favorable interactions with the enzyme, saturation of polar groups represents a necessary, but not sufficient, condition for high-affinity binding. Indeed, such interactions generally do little more than compensate for the energetic cost of stripping water molecules from these moieties. In order for very high affinity to be observed, there must be sufficient hydrophobic interactions. In the case of PheRS−OA, the phenyl group of OA is situated only shallowly within the hydrophobic pocket. Therefore, the low-energy conformation of PheRSTT−OA identified in our simulations does not contradict the experimental finding of millimolar to micromolar binding.

The residues within the binding site of PheRS are, not surprisingly, situated ideally to interact with FAMP, the natural substrate. More surprising is our finding that OA, despite the fact that it contains a Phe moiety, cannot bind in an analogous fashion, as has been hitherto assumed. We have found that OA can only bind in the active site in a significantly different conformation than FAMP (Figure 4). Furthermore, two alternative low-energy binding modes were identified which cannot be dismissed based on these simulations. Distinguishing between these possibilities will require much longer simulation times which include the entire tetrameric protein or additional experimental data, in the form of a crystal structure of the PheRS−OA complex or additional binding data for related compounds.

The lowest-energy conformations found for OA and OA^{2-} are virtually identical, as are the minimized energies. The results of a free-energy perturbation calculation point clearly to the monoanion as the ionization state with the higher affinity to PheRS, at least in this binding mode.

There exist significant differences in the primary sequence among PheRS from various species. Obviously, all the various PheRSs are capable of binding Phe and FAMP with high affinity.[45] Were OA to bind to PheRS completely analogously to the natural substrate, one might reasonably expect it to bind to the various PheRSs with comparable affinity. However, our results indicate a significant difference between the binding mode of FAMP and that of OA. In this case, there is no guarantee that the differences among PheRSs, which evidently do not preclude FAMP binding, do not disturb OA binding. Indeed, experimental inhibition by OA was observed for PheRS from *B. subtilis* and *S. cerevisiae*, but not for *E. coli*; data for *T. thermophilus* have not been reported. This discrepancy lends support to our finding that OA binds differently than FAMP.

It is not clear which residues determine whether the enzyme will be inhibited by OA. The residues lining the active site, including those directly engaged in the binding of OA in the conformers we have presented here, show high interspecies homology. The experimentally determined inhibition of PheRSBS, however, was weak; even slight changes distant from the active site might perturb the binding pattern enough to push the inhibition constant out of the detectable range. It may prove possible to pinpoint the crucial residues by means of homology modeling. In any case, the experimentally determined species discrepancy and the difference in the binding mode reported here both suggest that experimental results obtained with nonhuman PheRS may not be relevant in understanding human ochratoxicosis.[46]

It is important to point out that this caveat applies both to toxicological data and to computational results. The binding mode and affinity of OA to human PheRS (PheRSHS) may differ greatly from those to PheRSTT; thus, we cannot state with certainty that OA cannot bind strongly in a mode similar to FAMP in PheRSHS. Nevertheless, the findings presented here are noteworthy with respect to human ochratoxicosis for several reasons: (1) The purported importance of PheRS in ochratoxicosis rests on nonhuman data, largely bacterial. (2) The implication of PheRS as the target of OA in humans derived primarily from the phenylalanyl moiety in the latter; our finding that the phenylalanine moiety of OA cannot adopt the conformation of PheRS-bound FAMP calls this implication into question. (3) The demonstration that OA cannot bind analogously to FAMP in any organism is sufficient to warrant reinterpretation of this assumption in all species. Thus, while we have not disproven that PheRS is an important target of OA in humans, we have helped demonstrate that the assumptions and interpretations upon which this proposed mechanism rest must be reconsidered.

It has been reported by Creppy et al.[12] that OA analogues in which the phenylalanyl moiety has been replaced by other amino acids are also capable of inhibiting the respective aminoacyl-tRNA synthetases (aaRS), although OA−PheRS exhibited the highest degree of inhibition. Values of K_i ranged from 1.3 mM for PheRS−OA to 19 mM for the proline system (ProRS−proline-OA). Based on our results, which indicate significant differences in the binding mode of FAMP and OA to PheRS, it seems likely that the inhibition observed was not specific for each OA−aaRS system but, rather, that a number of OA analogues are capable of weakly inhibiting a variety of aaRSs. In fact, OA might

conceivably show higher affinity to other tRNA synthetases than it does to PheRS.

Conclusions

We have shown that the binding of OA to PheRS, contrary to previous assumptions, can hardly occur analogously to the binding of the natural substrate FAMP. Rather, OA must bind significantly more shallowly than FAMP and with the carbonyl and nitrogen moieties turned relative to the natural substrate. We have identified another low-energy conformation, in which the isocoumarin moiety occupies the hydrophobic pocket, which cannot be excluded on the basis of these studies. Additionally, a third, "loose" binding mode has been located; this mode does not appear much less favorable than the other two, "tight" modes and would explain the ability of aspartame to antagonize the inhibition of PheRS by OA without itself being toxic. However, it remains to be demonstrated that aspartame interacts directly with PheRS; until more concrete experimental data is available, the selective blocking by aspartame would seem to be mere speculation. Nonetheless, it is an intriguing concept which could conceivably be put to good use.

It has been suggested that all phenylalanine-metabolizing enzymes represent potential targets of OA.[47] OA has been shown to act as a substrate of phenylalanyl hydroxylase, for example.[48] The significant differences in the binding of OA and FAMP to PheRS, however, indicate that the inhibition of other Phe-metabolizing enzymes by OA cannot be assumed simply on the basis of OA's Phe moiety; whether OA is capable of inhibiting such enzymes depends on the actual topology of the binding site. Generally, the ammonium group of Phe can be expected to bind tightly to acidic and hydrogen-bond-accepting groups, if the energy of desolvating Phe is to be compensated for in the binding site, a requirement for strong binding. In PheRSTT, for example, the ammonium group is enclosed by His178, Ser180, and Glu220. The fact that the Phe moiety in OA bears no positive charge on the nitrogen, and that this group is substituted by the bulky isocoumarin moiety, suggests that enzymes which bind Phe strongly will generally be able to bind OA only after some reorganization. Crucial is the question of what the nature of the actual high-affinity substrate is, i.e., not necessarily Phe.

Our simulations suggest that the presence of a phenylalanyl moiety is not a necessary condition for antagonism. Therefore, it seems unlikely that searching for compounds with a phenylalanyl moiety as possible antagonists, such as aspartame, will be the quickest route to success. In fact, the two reports of ochratoxin antagonism, in one case by aspartame[16] and in the other by piroxicam,[17] are perhaps more straightforwardly interpretable based on the demonstrated influence of these agents on the plasma-binding properties of OA.[7] Thus, the most relevant interaction in preventing ochratoxicosis may well be not that with PheRS, but that with HSA. Fortunately, a number of pharmaceutical agents are known also to bind to HSA,[49] thus providing a large pool of prospective antagonists. These could be used directly or modified in order to tune their binding properties or decrease their intrinsic biological activity. For example, piroxicam, a potent antiinflammatory, might be altered in such a way as to maintain its plasma-binding properties yet decrease the side effects which one might expect at the doses administered in Baudrimont et al.'s study. Using the three-dimensional structure of HSA, we are currently continuing our investigation of its interactions with OA and some candidate antagonists.

Acknowledgment. We are grateful to Prof. Mark Safro (Weizmann Institute, Rehovot, Israel) for making the structure of PheRSTT available to us prior to release in the Brookhaven Protein Data Bank and to Dr. Arend Bruinink (ETH, Zürich, Switzerland) for sharing toxicity data prior to publishing. We thank Prof. Peter Maier (ETH and Universität Zürich, Switzerland) for helpful discussions. This work was made possible by the generous support of the 3R Research Foundation, Switzerland (Grant 55-96), and the Swiss National Science Foundation (Grant 3100-052237.97).

Note Added in Proof. Subsequent to submission of this manuscript, the crystal structure of PheRS from *T. thermophilus* complexed with phenylalaninyl adenylate (PheOH-AMP), an analogue of FAMP, was published (Reshetnikova, L.; Moor, N.; Lavrik, O.; Vassylyev, D. G. *J. Mol. Biol.* **1999**, *287*, 555−568). While the overall binding mode of PheRS−FAMP described here is in good agreement with the complex with PheOH-AMP described by Reshetnikova et al., the induced fit observed by those workers, specifically the shift of the motif 2 loop and the associated motion of R321, was not identified by our simulations, which considered only a zone of the entire protein due to computational limits. The binding of the phenylalanine moiety of FAMP described here is thus in excellent agreement with the experimental structure, whereas the specific contacts of the adenine moiety and ribose ring show only partial agreement. Particularly, the contact between E206 and the adenine group was found but not those between the adenine and E213. However, the analogue, PheOH-AMP, lacks the carbonyl group which in the natural substrate is situated to form a hydrogen bond with W149 as well as with Q183, which can thus bridge the carbonyl oxygen and the ribose O5. Furthermore, the protonation state of H178 in the complex with PheOH-AMP was not discussed by Reshetnikova et al. The ϵ-protonated tautomer is able to bridge the ammonium of FAMP and the backbone carbonyl group of N133, whereas the δ-protonated tautomer, which acts as a hydrogen-bond donor in the complex of PheRS with phenylalanine, makes no strong hydrogen bonds in the complex with PheOH-AMP.

References

(1) Pohland, A. E.; Nesheim, S.; Friedman, L. Ochratoxin A: A Review. *Pure Appl. Chem.* **1992**, *64*, 1029−1046.
(2) Marquart, R. R.; Fröhlich, A. A. A Review of Recent Advances in Understanding Ochratoxicosis. *J. Anim. Sci.* **1992**, *70*, 3968−3988.
(3) Hult, K.; Plestina, R.; Habazin-Novak, V.; Radic, B.; Ceovic, S. Ochratoxin A in Human Blood and Balkan Endemic Nephropathy. *Arch. Toxicol.* **1982**, *51*, 313−321.
(4) Abbreviations: OA, ochratoxin A {(*R*)-*N*-[(5-chloro-3,4-dihydro-8-hydroxy-3-methyl-1-oxo-1*H*-2-benzopyran-7-yl)carbonyl]-L-phenylalanine}; Phe, L-phenylalanine; PheRS, phenylalanyl-tRNA synthetase; PheRSBS, PheRS from *B. subtilis*; PheRSEC, PheRS from *E. coli*; PheRSSC, PheRS from *S. cerevisiae*; PheRSTT, PheRS from *T. thermophilus*; FAMP, phenylalanyl adenylate; HSA, human serum albumin.
(5) Chu, F. S. Studies on Ochratoxins. *CRC Crit. Rev. Toxicol.* **1974**, *2*, 499−524.
(6) Pitout, M. J. The Effect of Ochratoxin A on Glycogen Storage in the Rat Liver. *Toxicol. Appl. Pharmacol.* **1968**, *13*, 299−306.
(7) Galtier, P. Pharmacokinetics of Ochratoxin A in Animals. *IARC Sci. Publ.* **1991**, *115*, 187−200.
(8) van der Merwe, K. J.; Steyn, P. S.; Fourie, L.; Scott, B.; Theron, J. J. Ochratoxin A, a Toxic Metabolite Produced by *Aspergillus ochraceus* Wilh. *Nature* **1965**, *205*, 1112−1113.

(9) Konrad, I.; Röschenthaler, R. Inhibition of Phenylalanine tRNA Synthetase from *Bacillus subtilis* by Ochratoxin A. *FEBS Lett.* **1977**, *83*, 341−347.
(10) Significant differences exist in the primary sequences of tRNA synthetases from various species (ref 11); the homology between PheRSEC and PheRSBS, specifically, is only 40%. The active site shows higher homology but still displays numerous differences which may be relevant in the binding of OA.
(11) Arnez, J. G.; Moras, D. Structural and functional considerations of the aminoacylation reaction. *Trends Biochem. Sci.* **1997**, *22*, 211−216.
(12) $$\% \text{ inhibition} = 100 \times \frac{[I]}{K_i\left(1 + \frac{[S]}{K_m}\right)}$$
This equation is valid for competitive inhibition; see: Creppy, E. E.; Kern, D.; Steyn, P. S.; Vleggar, R.; Röschenthaler, R.; Dirheimer, G. Comparative Study of the Effects of Ochratoxin A Analogues on Yeast Phenylalanyl tRNA-synthetase and on the Growth and Protein Synthesis of Hepatoma Cells. *Toxicol. Lett.* **1983**, *19*, 217−224.
(13) Roth, A.; Eriani, G.; Dirheimer, G.; Gangloff, J. Kinetic properties of pure overproduced *Bacillus subtilis* phenylalanyl-tRNA synthetase do not favour its in vivo inhibition by ochratoxin A. *FEBS Lett.* **1993**, *326*, 87−91.
(14) Bruinink, A.; Rasonyi, T.; Sidler, C. Reduction of ochratoxin A toxicity by heat-induced epimerization. In vitro effects of ochratoxins on embryonic chick meningeal and other cell cultures. *Toxicology* **1997**, *118*, 205−210.
(15) Creppy, E. E.; Stormer, F. C.; Kern, D.; Röschenthaler, R.; Dirheimer, G. Effects of Ochratoxin A Metabolites on Yeast Phenylalanyl-tRNA Synthetase and on the Growth and In Vivo Protein Synthesis of Hepatoma Cells. *Chem.-Biol. Interact.* **1983**, *47*, 217−224.
(16) Baudrimont, I.; Betbeder, A. M.; Creppy, E. E. Reduction of the ochratoxin A-induced cytotoxicity in Vero cells by aspartame. *Arch. Toxicol.* **1997**, *71*, 290−298.
(17) Baudrimont, I.; Murn, M.; Betbeder, A. M.; Guilcher, J.; Creppy, E. E. Effect of piroxicam on the nephrotoxicity induced by ochratoxin A in rats. *Toxicology* **1995**, *95*, 147−154.
(18) Hagelberg, S.; Hult, K.; Fuchs, R. Toxicokinetics of Ochratoxin A in Several Species and its Plasma-binding Properties. *J. Appl. Toxicol.* **1989**, *9*, 91−96.
(19) Kumagai, S. Ochratoxin A: Plasma Concentration and Excretion into Bile and Urine in Albumin-Deficient Rats. *Food Chem. Toxicol.* **1985**, *23*, 941−943.
(20) Goldgur, Y.; Mosyak, L.; Reshetnikova, L.; Ankilova, V.; Larik, O.; Khodyreva, S.; Safro, M. The crystal structure of phenylalanyl-tRNA synthetase from *Thermus thermophilus* complexed with cognate $tRNA^{Phe}$. *Structure* **1997**, *5*, 59−68.
(21) Mohamadi, F.; Richards, N. G. J.; Guida, W. C.; Liskamp, R.; Lipton, M.; Caufield, C.; Chang, G.; Hendrickson, T.; Still, W. C. MacroModel − An Integrated Software System for Modeling Organic and Bioorganic Molecules Using Molecular Mechanics. *J. Comput. Chem.* **1990**, *11*, 440−467.
(22) Still, W. C.; Tempczyk, A.; Hawley, R. C.; Hendrickson, T. Semianalytical Treatment of Solvation for Molecular Mechanics and Dynamics. *J. Am. Chem. Soc.* **1990**, *112*, 6127−6129.
(23) Weiner, S. J.; Kollman, P. A.; Case, D. A.; Singh, U. C.; Ghio, C.; Alagona, G.; Profeta, S., Jr.; Weiner, P. A New Force Field for Molecular Mechanical Simulation of Nucleic Acids and Proteins. *J. Am. Chem. Soc.* **1984**, *106*, 765−784.
(24) Besler, B. H.; Merz, K. M., Jr.; Kollman, P. A. Atomic Charges Derived from Semiempirical Methods. *J. Comput. Chem.* **1990**, *11*, 431−439.
(25) Stewart, J. J. P. MOPAC − A Semiempirical Molecular Orbital Program. *J. Comput.-Aided Mol. Des.* **1990**, *4*, 1−105.
(26) Although the partial charges vary slightly with the conformation used to calculate them, the conformer found to have the lowest energy was the same regardless of which conformer was used to calculate the partial charge set. Recalculation of the partial charges using the conformation adopted in the complex with PheRS had only a negligible effect on the final minimized structure.
(27) Bernstein, F. C.; Koetzle, T. F.; Williams, J. G. B.; Meyer, E. F., Jr.; Brice, M. R.; Rodgers, J. R.; Kennard, O.; Shimanouchi, T.; Tasumi, M. The Protein Data Bank: A Computer-based Archival File for Macromolecular Structures. *J. Mol. Biol.* **1977**, *112*, 535−542.
(28) (a) Vedani, A.; Huhta, D. W. A New Force Field for Modeling Metalloproteins. *J. Am. Chem. Soc.* **1990**, *112*, 4759−4767. (b) Zbinden, P.; Dobler, M.; Folkers, G.; Vedani, A. PrGen: Pseudoreceptor Modeling Using Receptor-mediated Ligand Alignment and Pharmacophore Equilibration. *Quant. Struct.-Act. Relat.* **1998**, *17*, 122−130. (c) Vedani, A.; Zbinden, P.; Snyder, J. P.; Greenidge, P. A. Pseudoreceptor Modeling: The Construction of Three-Dimensional Receptor Surrogates. *J. Am. Chem. Soc.* **1995**, *117*, 4987−4994.
(29) (a) Preliminary molecular dynamics studies treated the entire α-subunit, including all degrees of freedom, but neglecting $tRNA^{Phe}$ and the β-subunit. During the dynamics simulation, large changes in the three-dimensional structure of the enzyme were observed. Apparently, the influence of the other three subunits of the tetramer is decisive in determining the tertiary structure of PheRS. (b) Branchini, B. R.; Nemser, A. R.; Zimmer, M. A Computational Analysis of the Unique Protein-Induced Tight Turn That Results in Posttranslational Chromophore Formation in Green Fluorescent Protein. *J. Am. Chem. Soc.* **1998**, *120*, 1−6.
(30) Guarnieri, F.; Still, W. C. A Rapidly Convergent Simulation Method: Mixed Monte Carlo/Stochastic Dynamics. *J. Comput. Chem.* **1994**, *15*, 1302−1310.
(31) Eriani, G.; Delarue, M.; Poch, O.; Gangloff, J.; Moras, D. Partition of tRNA synthetases into two classes based on mutually exclusive sets of sequence motifs. *Nature* **1990**, *347*, 203−206.
(32) Arnez, J. G.; Augustine, J. G.; Moras, D.; Francklyn, C. S. The first step of aminoacylation at the atomic level in histidyl-tRNA synthetase. *Proc. Natl. Acad. Sci. U.S.A.* **1997**, *94*, 7144−7149.
(33) Onesti, S.; Miller, A. D.; Brick, P. The crystal structure of the lysyl-tRNA synthetase (LysU) from *Escherichia coli*. *Structure* **1995**, *3*, 163−176.
(34) Baltzinger, M.; Lin, S. X.; Remy, P. Yeast Phenylalanyl-tRNA Synthetase: Symmetric Behavior of the Enzyme during Activation of Phenylalanine As Shown by a Rapid Kinetic Investigation. *Biochemistry* **1983**, *22*, 675−681.
(35) Ibba, M.; Kast, P.; Hennecke, H. Substrate Specificity is Determined by Amino Acid Binding Pocket Size in *Escherichia coli* Phenylalanyl-tRNA Synthetase. *Biochemistry* **1994**, *33*, 7107−7112.
(36) Ibba, M.; Hennecke, H. Relaxing the substrate specificity of an aminoacyl-tRNA synthetase allows in vitro and in vivo synthesis of proteins containing unnatural amino acids. *FEBS Lett.* **1995**, *364*, 272−275.
(37) Ponder, J. W.; Richards, F. M. Tertiary Templates for Proteins: Use of Packing Criteria in the Enumeration of Allowed Sequences for Different Structural Classes. *J. Mol. Biol.* **1987**, *193*, 775−791.
(38) McCammon, J. A.; Harvey, S. C. *Dynamics of Proteins and Nucleic Acids*; Cambridge University Press: Cambridge, 1987; p 71.
(39) van Gunsteren, W. F.; Mark, A. E. On the interpretation of biochemical data by molecular dynamics computer simulation. *Eur. J. Biochem.* **1992**, *204*, 947−961.
(40) (a) Doster, R. C.; Sinnhuber, R. O. Comparative Rates of Hydrolysis of Ochratoxin A and B In Vitro. *Food Cosmet. Toxicol.* **1972**, *10*, 389−394. (b) Preliminary simulations of the binding of OA to bovine carboxypeptidase A (BCPA) using Yeti metalloprotein modeling software[28a] suggest that OA binds with the amide oxygen atom bound to the catalytic Zn atom of BCPA and the carboxylate group bound to Arg145, analogously to the crystallographically determined binding mode of the BCPA inhibitor l-benzylsuccinic acid (B. Galliker, A. Vedani, unpublished results).
(41) Carter, D. C.; Ho, J. X. Structure of Serum Albumin. *Adv. Protein Chem.* **1994**, *45*, 153−203.
(42) Stojkovic, R.; Hult, K.; Gamulin, S.; Plestina, R. High Affinity Binding of Ochratoxin A to Plasma Constituents. *Biochem. Int.* **1984**, *9*, 33−38.
(43) Bruinink, A.; Sidler, C. The Neurotoxic Effects of Ochratoxin-A are Reduced by Protein Binding but Are Not Affected by *l*-Phenylalanine. *Toxicol. Appl. Pharmacol.* **1997**, *146*, 173−179.
(44) He, X. M.; Carter, D. C. Atomic structure and chemistry of human serum albumin. *Nature* **1992**, *358*, 209−215.
(45) While the amino acid substrate (FAMP) is identical for PheRS in all species, the cognate tRNA is not. Further, the importance of proofreading in translation fidelity has been reported to increase during evolution (Gabius, H.-J.; von der Haar, F.; Cramer, F. Evolutionary Aspects of Accuracy of Phenylalanyl-tRNA Synthetase. A Comparative Study with Enzymes from *Escherichia coli*, *Saccharomyces cerevisiae*, *Neurospora crassa*, and Turkey Liver using Phenylalanine Analogues. *Biochemistry* **1983**, *22*, 2231−2339). Differences in sequence are therefore likely to serve tRNA recognition and proofreading mechanisms.
(46) It is interesting to note in this regard that of all those residues directly involved in binding, only one is conserved between *B. subtilis* and *S. cerevisiae* (which showed inhibition by OA) yet different for *E. coli* (which showed no inhibition), namely at the position corresponding to Trp149 in *T. thermophilus*, which is a His in *E. coli* but a Gln in *B. subtilis* and *S. cerevisiae*. This residue is also occupied by His in the putative human PheRS.

(47) Dirheimer, G.; Creppy, E. E. Mechanism of Action of Ochratoxin A. *IARC Sci. Publ.* **1991**, *115*, 171−186.
(48) Creppy, E. E.; Chakor, K.; Fisher, M. J.; Dirheimer, G. The mycotoxin ochratoxin A is a substrate for phenylalanine hydroxylase in isolated rat hepatocytes and in vivo. *Arch. Toxicol.* **1990**, *64*, 279−284.
(49) Kragh-Hansen, U. Molecular Aspects of Ligand Binding to Serum Albumin. *Pharmacol. Rev.* **1981**, *33*, 17−53.
(50) Sayle, R.; Milner-White, E. J. RasMol: Biomolecular graphics for all. *Trends Biochem. Sci.* **1995**, *20*, 374.

JM991040K